Product Whitepaper: Accelerated Lifetime Testing System for Photovoltaics

Ark Metrica

sales@arkmetrica.com

December 11, 2025

1. INTRODUCTION

Photovoltaic devices based on emerging materials, such as perovskites, must maintain high performance for many years in the real world if they are to make a significant contribution to meeting a growing global energy demand. However, stabilising emerging materials for use in real world conditions has proven to be a significant research challenge. In the field, devices are exposed to sunlight, heat, electrical load, oxygen, and moisture, all of which can cause the constituent materials to degrade, leading to reductions in device performance over time. Understanding the fundamental causes of these effects, and devising and testing strategies to mitigate them, is therefore critical.

There are several technical challenges that make rapid stability testing difficult in research labs. Historically, it has simply been slow work: it takes time to degrade a samples using conventional tools. Furthermore, conventional stability testing based on IEC [1] and ISOS [2] protocols typically focusses on each stressor individually. While this is useful, stressors may compound. This approach may therefore fail to expose important degradation pathways that emerge when stressors are combined. In addition, integrated testing systems are not readily commercially available, leading research groups to spend significant effort building their own ad-hoc systems from relatively expensive components.

To address these issues, a commercially-applicable accelerated lifetime testing system for photovoltaics has been developed. The system is built using a new low-cost, simplified, high-intensity light emitting diode (LED) light engine; a custom environment chamber and atmosphere conditioning system; a new low-cost source-measurement unit (SMU) for electrical biasing and characterisation that can scale to high channel counts; and employs robust, automated, in-situ data collection. Combined, this system provides high simultaneous stresses on devices, with high throughput measurements, at low cost, making fast stability testing more accessible to the research community. This white paper discusses this system in detail.

2. LIGHT ENGINE

The custom-built light engine aims to be low-cost, high intensity, stable, uniform over large areas, and have a broadband spectrum with ultraviolet (UV) and infrared (IR) components that offer low spectral mismatch compared to AM1.5G.

The metal-core printed circuit board (PCB) design for the LED sub-arrays, shown in Figure 2.1, is based on a square tileable unit that can tile the plain whilst maintaining the LED pitch, ensuring uniformity over any required area.

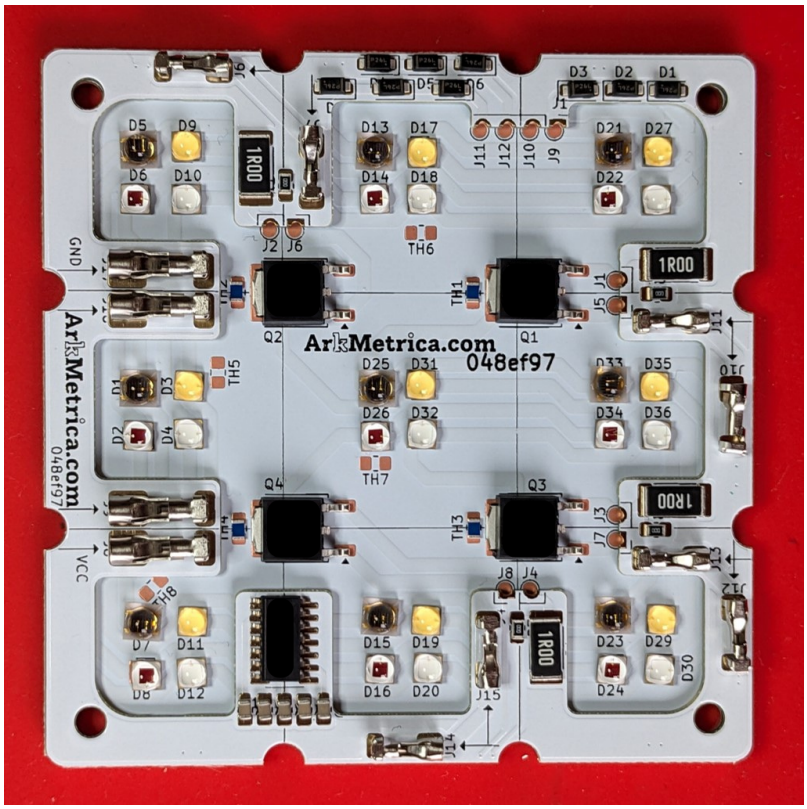

Figure 2.1: Photograph of the tileable LED sub-array.

The LED colour channels have been carefully chosen to produce a broadband spectrum, shown in Figure 2.2a, with UV and IR components that offer a Class C spectral mismatch (IEC 60904-9:2020 exteneded wavelength range [3]) compared to AM1.5G, as shown in Figure 2.2c. This has been achieved with just four LED channels, reducing the complexity of the driving circuitry compared to conventional LED solar simulators, minimising the cost. The available irradiance from the LED array of >2 suns equivalent enables faster degradation of devices for higher throughput aging studies.

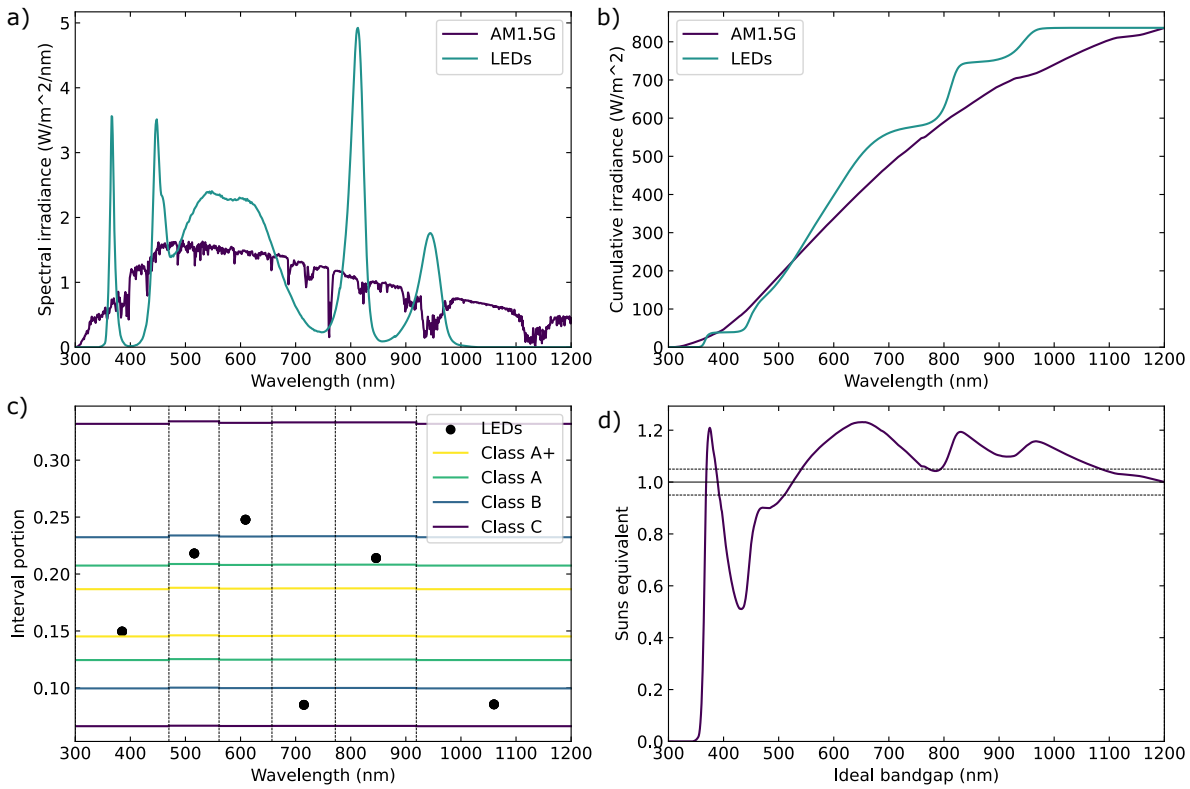

Figure 2.2: Simulated optical properties of the LED light engine compared to AM1.5G: (a) spectral irradiance, (b) integrated irradiance, (c) proportion of irradiance in each spectral band (IEC 60904-9:2020 [3]), and (d) spectrally resolved equivalent number of suns as a function of ideal step-function bandgap when aiming for 1 sun equivalent.

The tiled LED arrangement offers good uniformity and optical throughput within the area of the tiled array when coupled with mirror walls, as shown in Figure 2.3. Class B or higher uniformity is achieved over the entire 21.6 cm $\times$ 21.6 cm area, Class A over 16.8 cm $\times$ 16.8 cm, and Class A+ over 10.7 cm $\times$ 10.7 cm [3].

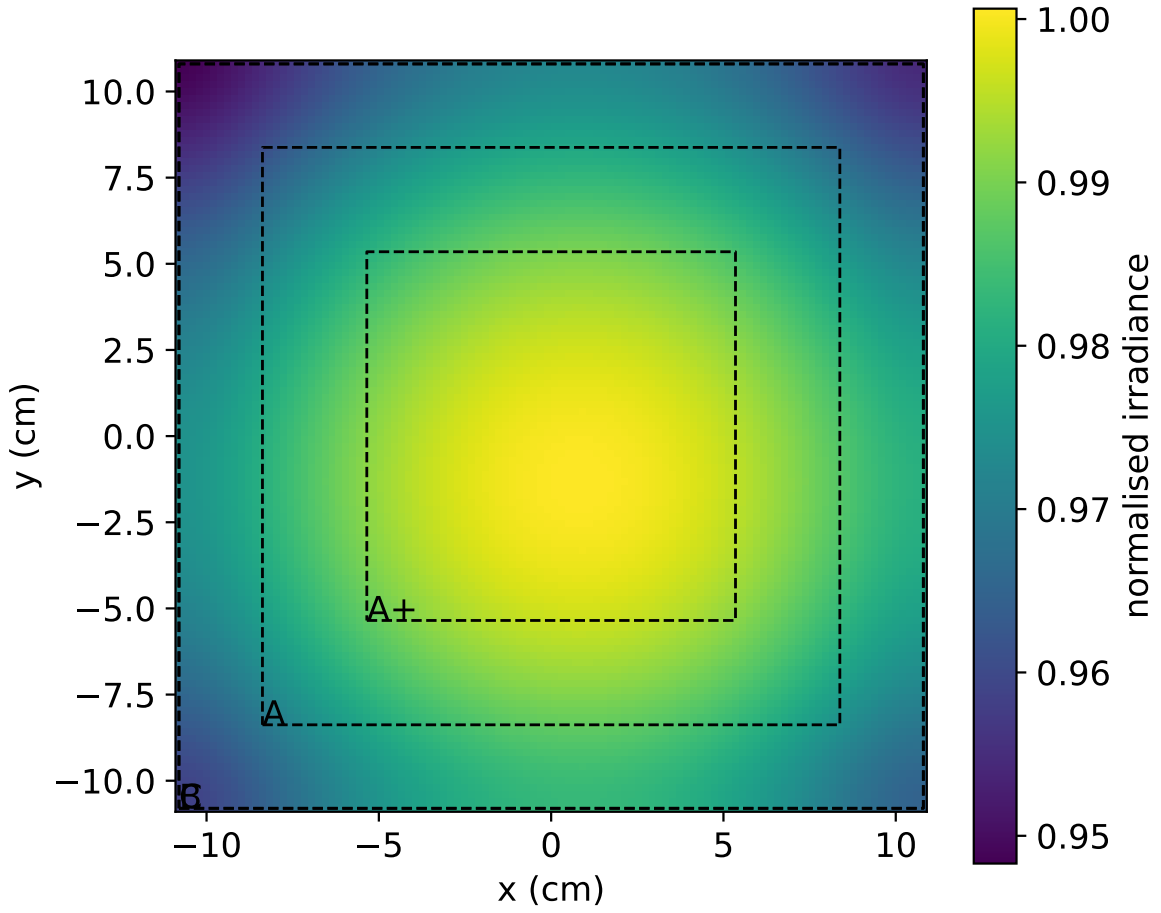

Figure 2.3: Simulated normalised irradiance of the LED light engine with mirror walls. Dashed lines and letters indicate regions of the given Class of uniformity [3].

The light engine is driven with a newly developed current sourcing circuit with excellent temporal stability, as shown in Figure 2.4. The drivers allow control of the intensity of each individual LED channel allowing further improvements to spectral mismatch when illuminating photovoltaic devices based on absorbers with specific bandgaps.

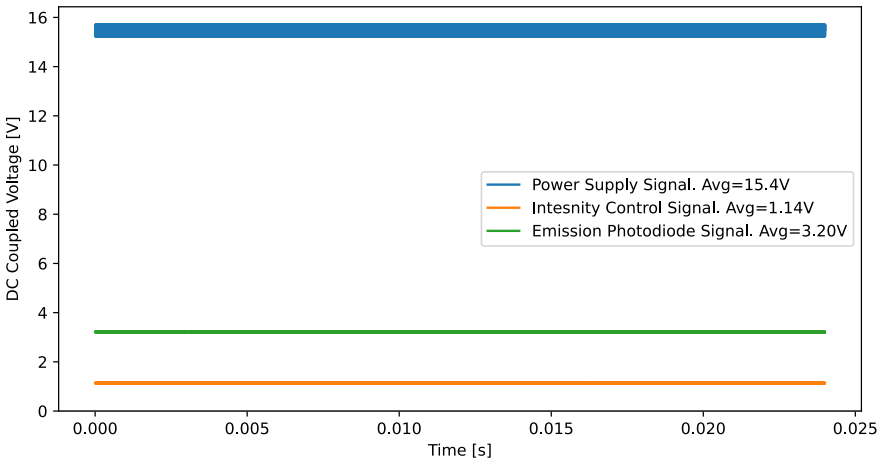

Figure 2.4: Temporal stability of LED output when driven with the custom current sourcing circuit, as measured with a Si photodiode.

3. ENVIRONMENT CHAMBER AND ATMOSPHERE CONTROL

To vary the environmental stressors on devices during degradation studies, the samples are housed inside a custom-built chamber, shown with the lid removed in Figure 3.1. Gas fittings in the walls allow gases of controlled composition to flow through the chamber, controlling its atmosphere. The chamber features an array of pockets for mounting substrates, each with an array of pogo-pins for making electronic contact to devices. Channels have been removed from the sample holder to allow the gas flow controlling the atmospheric composition to pass directly over the surface of the devices. The electronic contacts are passed through the wall of chamber and sealed with a silicone sealant. The feedthroughs, lid, and screws are all o-ring sealed for optimal control of the internal atmosphere. The lid features a fused-silica window to seal the chamber whilst enabling light, including UV, to reach the devices.

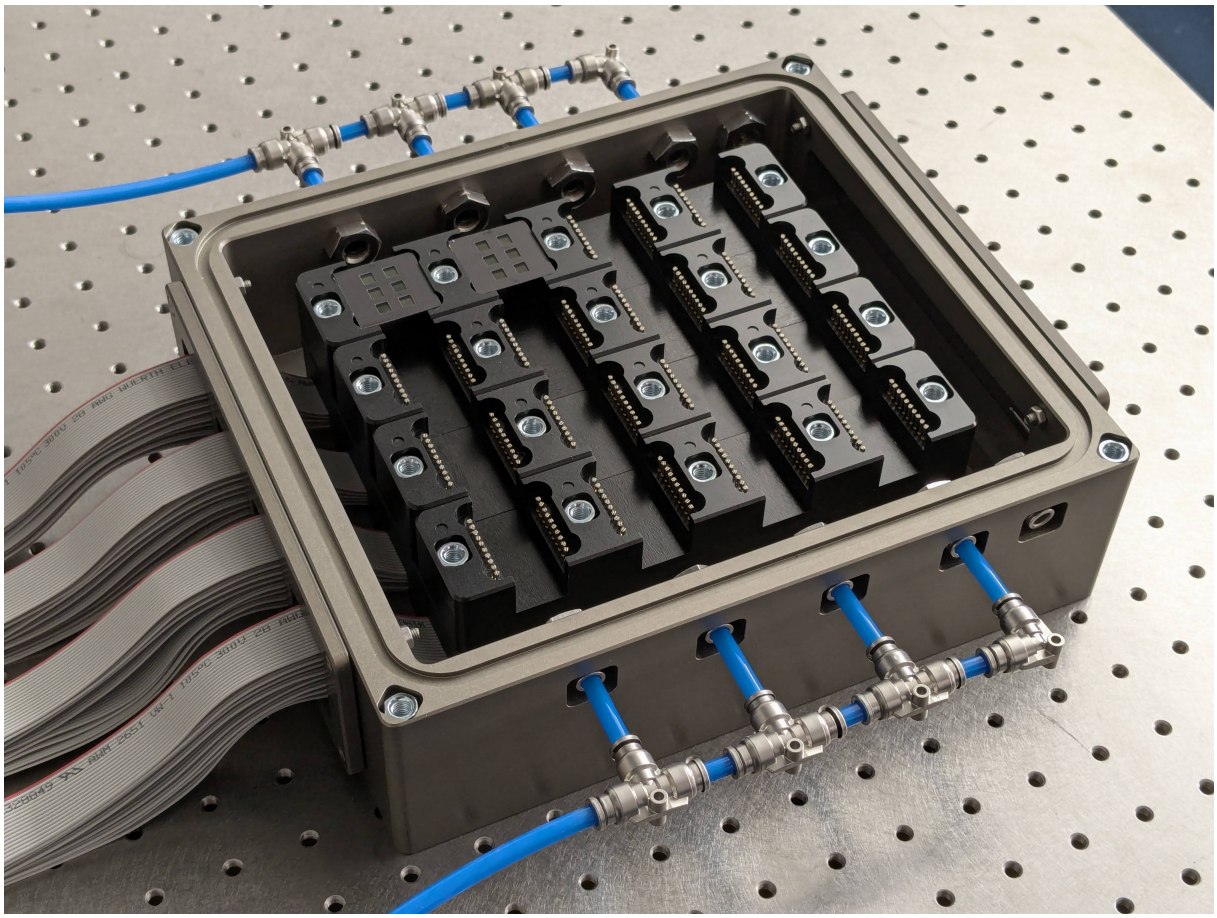

Figure 3.1: Open environment chamber showing mounted devices, pogo pin array, and gas flow channels.

Control of the temperature of the metallic chamber is achieved by placing it on a hotplate under the LED array as shown in Figure 4.3. This minimises water condensation on the walls of the chamber when warm humid gas flows through it. The substrate temperature is influenced by the light intensity, chamber wall temperature, and gas temperature, all of which can be user-controlled and tuned according to the requirements of the experiment.

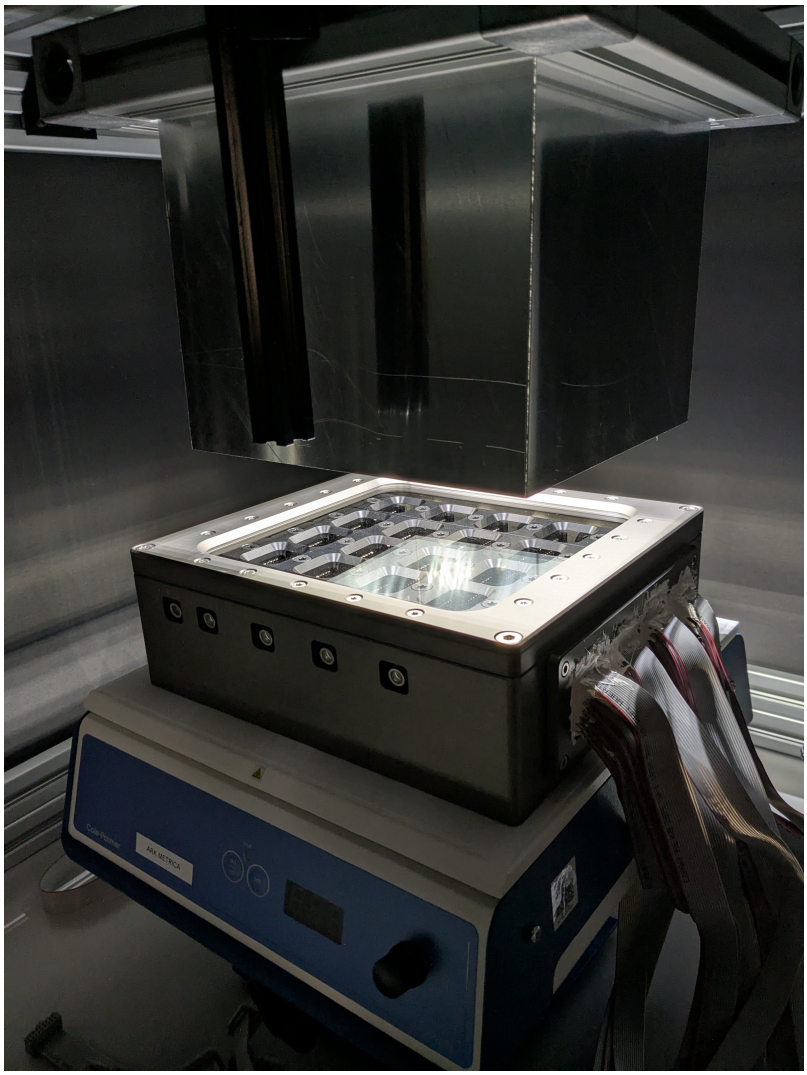

Figure 3.2: Environment chamber mounted on a hotplate under the LED array with mirrored walls for improved uniformity.

A humidity controller based on the open-source OpenHumidistat [4] is used to control humidity in the environment chamber in the range 10–85 %RH. A schematic of the control system is shown in Figure 3.3.

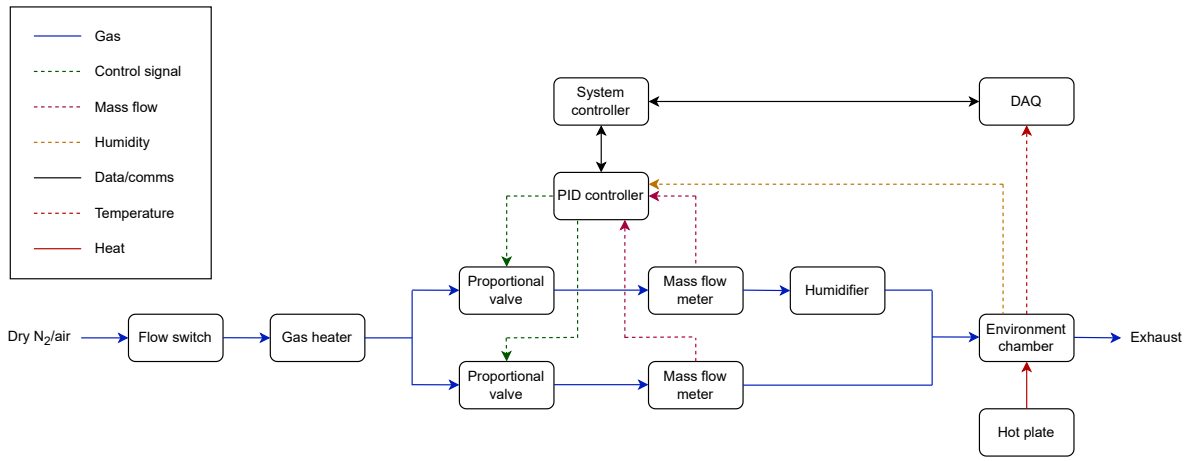

Figure 3.3: Schematic of control and monitoring of the environment inside the environment chamber.

In brief, a dry air or nitrogen (with or without O_2 stress, respectively) gas flow is heated with a gas heater; split into two lines: one dry, one humid; and recombined before flowing through the environment chamber. The humidity in the chamber is controlled by variating the ratio of mass flow in each of the split lines using proportional solenoid valves controlled by a proportional-integral-derivative (PID) feedback loop, which reads humidity from a sensor in the environment chamber. The humidifier is a gas bubbler. The temperature and humidity inside the chamber can be logged to the system controller (see Section 5). The solenoids, mass flow meters, and PID controller are housed securely in an enclosure, shown in Figure 3.4.

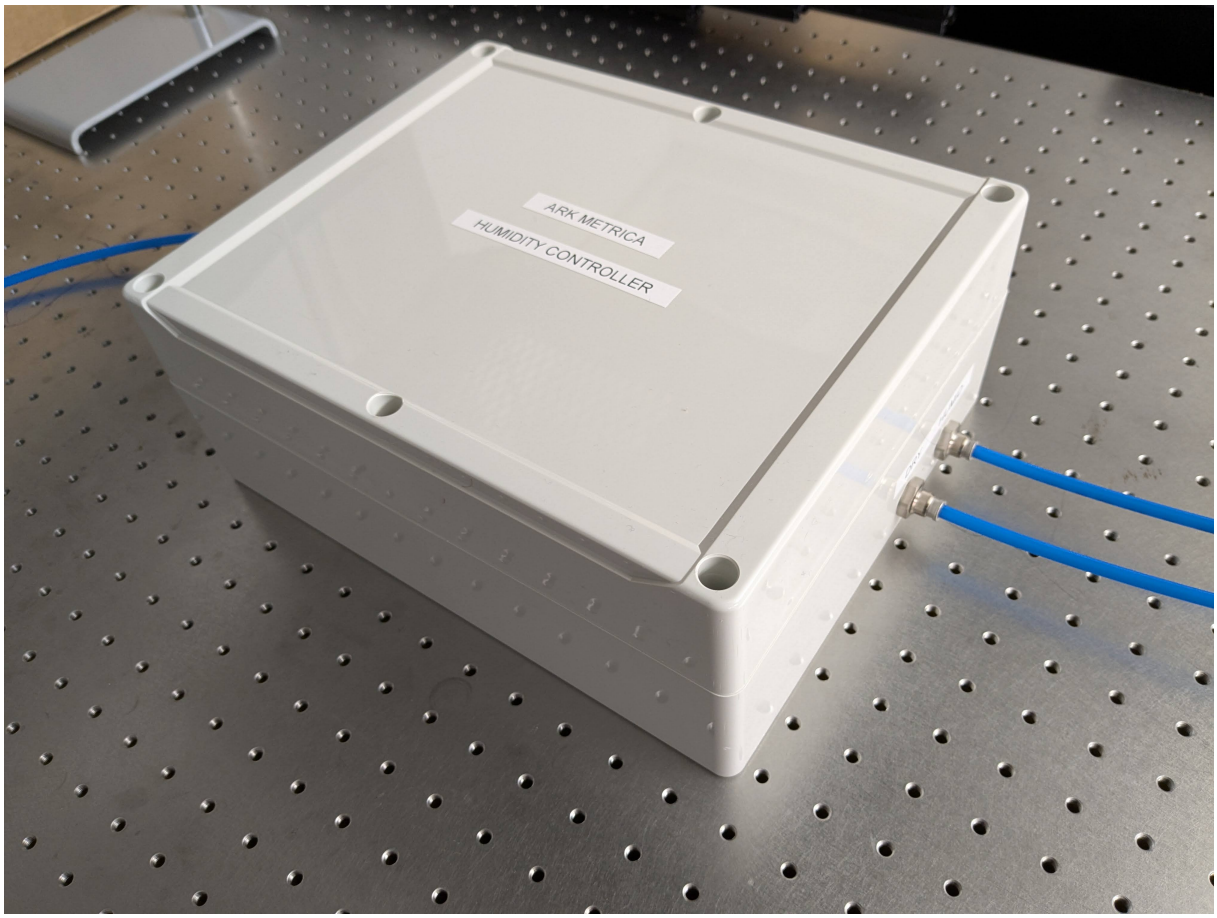

Figure 3.4: Humidity control box with inlet and outlet gas connections.

An example measurement run shown in Figure 3.5 demonstrates that reaching the target setpoint following step changes at various humidity levels can be achieved within a few minutes.

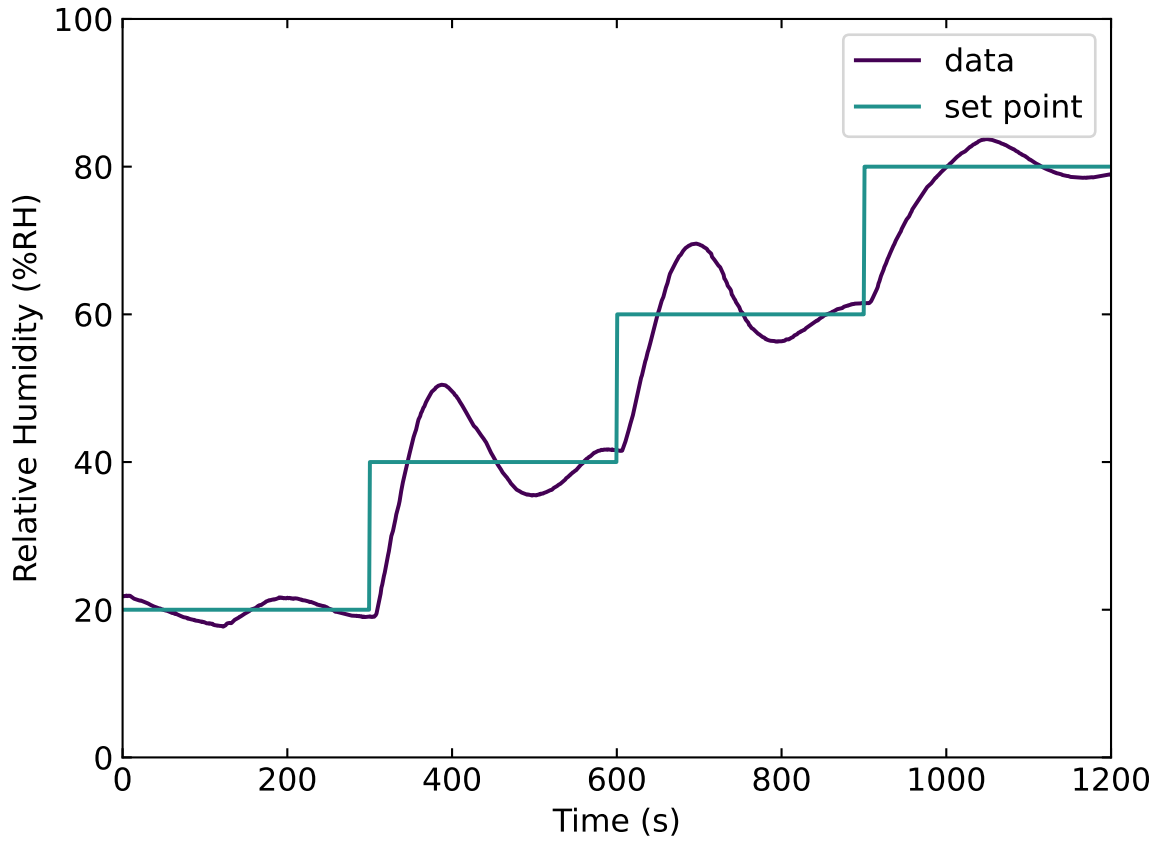

Figure 3.5: Humidity control at various setpoints as a function of time.

4. SOURCE-MEASUREMENT UNIT

The custom-built SMU, shown in Figure 4.1, is designed to provide a sufficient specification for the measurement of research-scale devices but with a significantly lower cost-per-channel than a conventional SMU. This is critical to scaling in-situ device control/monitoring to high channel counts, allowing higher measurement throughput. Each unit has the following specifications:

- Number of independent channels: 4
- Voltage range: ± 5 V
- Voltage DAC set resolution: 16-bit
- Voltage ADC measure resolution: 16-bit
- Current range: ± 0.2 A
- Current DAC set resolution: 16-bit
- Current ADC measure resolution: 16-bit
- Interfaces: RJ45 (10/100BT)

- IP configuration: DHCP
- Programming: Custom command set based on a subset of SCPI
- Power supply: 12 VDC, 1.6A

Figure 4.1: 4-channel SMU.

The channels that comprise each SMU are fully independent allowing simultaneous control and measurement of four devices. Some example lifetime testing data obtained from the parallel measurement of four perovskite solar cells with a single SMU is shown in Figure 4.2. Here the devices are nominally controlled and monitored with maximum power-point tracking (MPPT) using a gradient descent algorithm. Periodically, the devices undergo a scan routine comprised of: open-circuit voltage (V_{OC}) vs. time, current density-voltage (J-V), and short-circuit current density (J_{SC}) vs. time, before returning back to MPPT. This provides a greater insight into any changes in the operation of the devices during their degradation than a simple measurement of MPPT can provide alone.

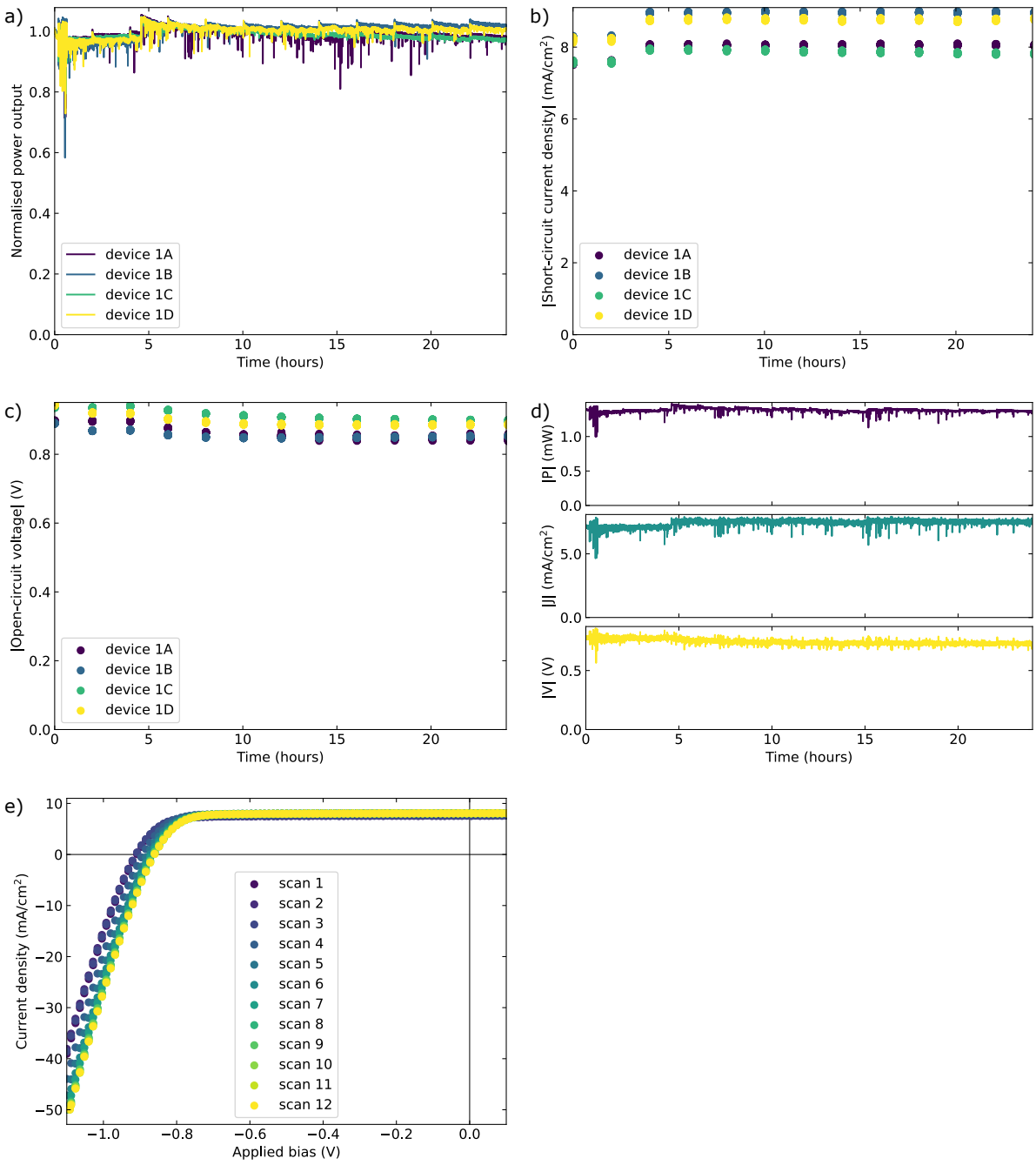

Figure 4.2: Simultaneous measurements of four devices using the SMU: (a) normalised maximum power output vs. time, (b) J_{SC} vs. time, (c) V_{OC} vs. time, (d) example maximum power output, voltage, and current density vs. time for a device, and (e) example J-V curves measured periodically for a device

In the present system there are eight SMUs for a total of 32 channels. The units have been designed to be compatible with standard 19" racking, as shown in Figure 4.3. This allows the simultaneous control and measurement of up to two devices per substrate on each of the 16 substrates that can be mounted in the environment chamber.

Figure 4.3: System photograph showing enclosed lightsource, 32 rack mounted SMU channels, and the control computer.

5. CONTROLLER

Experiments are automated with an extended version of the open-source control software developed at the University of Oxford [5]. Its graphical user interface (GUI), shown in Figure 5.1, allows for easy customisation of the measurement routine using the hardware developed for the accelerated lifetime testing system.

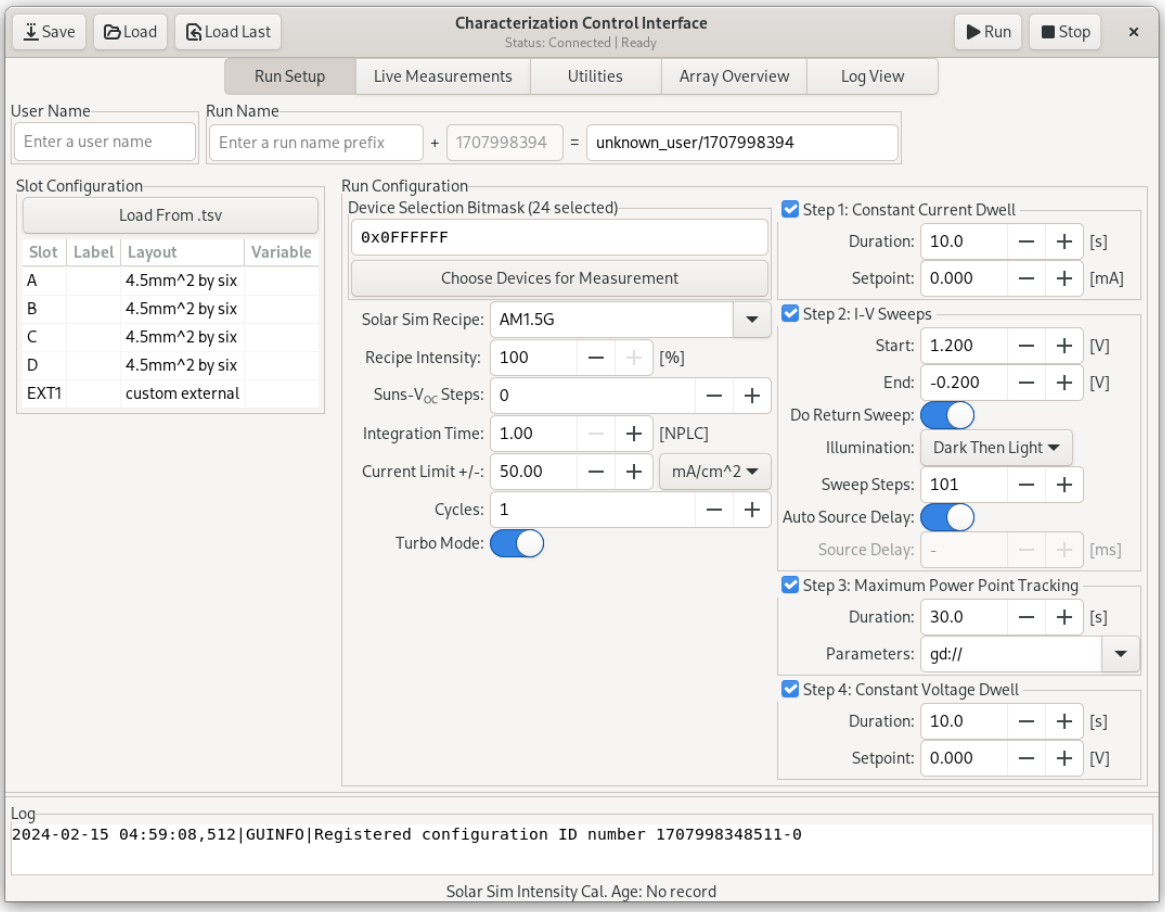

Figure 5.1: GUI for measurement configuration.

This runs on a robust industrial computer, shown in Figure 5.2, configured with data storage in a redundant array of independent disks (RAID), adding a high level of data integrity.

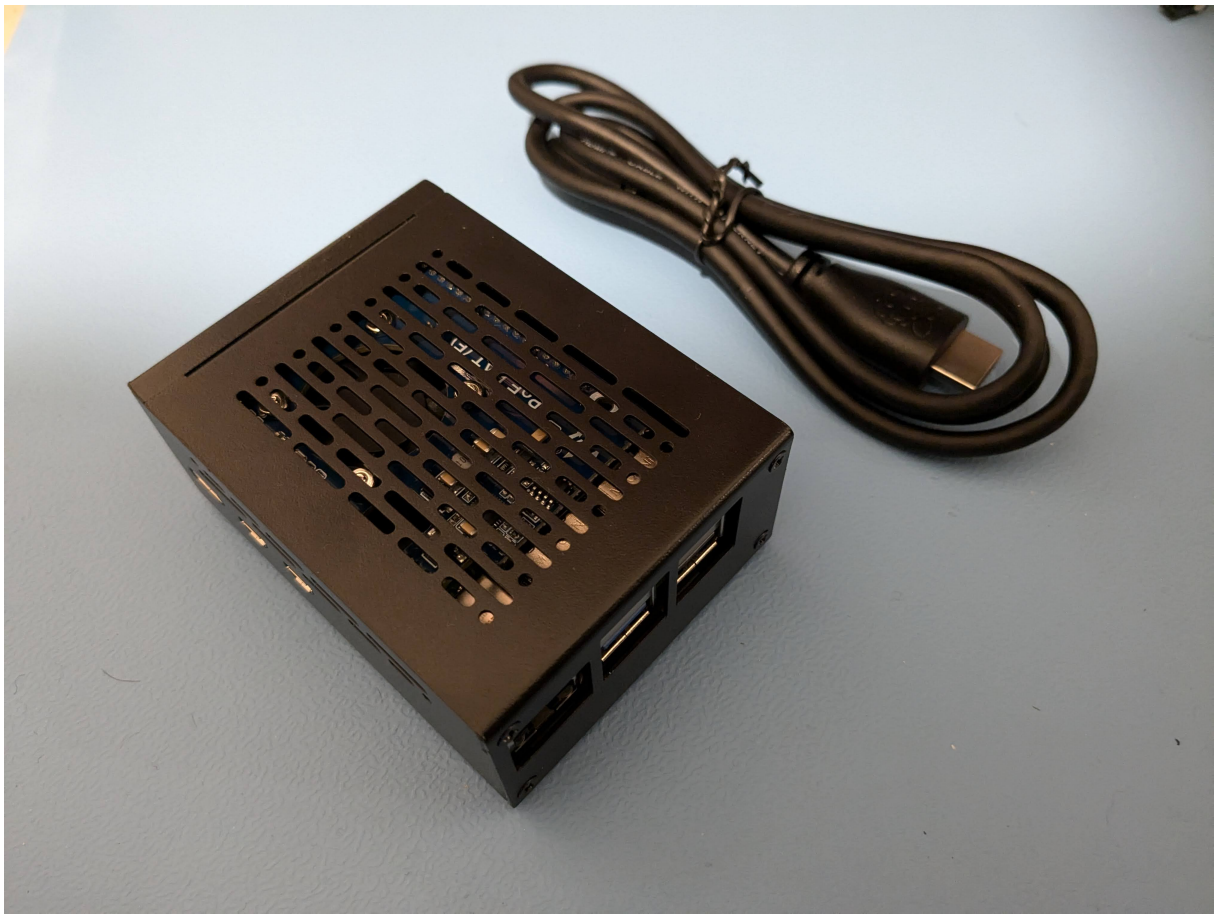

Figure 5.2: System controller with RAID.

6. SUMMARY

A new accelerated lifetime testing system for photovoltaics has been developed. The system is comprised of an LED light engine; an environment chamber with atmosphere control; a scalable SMU; and a mechanism for robust, automated, in-situ data collection. These components have been designed with low cost in mind to provide researchers with a fast, reliable, and accessible tool for studying the stability of photovoltaic devices based on emerging materials.

7. COMMERCIAL AVAILABILITY

Contact sales@arkmetrica.com for availability and pricing.

8. ACKNOWLEDGEMENTS

Ark Metrica Ltd. acknowledge funding from the European Union's Horizon Europe research and innovation program under grant agreement no. 101082176 - VALHALLA. We also thank Dr. Barkha Tyagi for providing devices for measurement.

REFERENCES

[1] International Electrotechnical Commission, “IEC 61215: Terrestrial Photovoltaic (PV) Modules - Design Qualification and Type Approval,” 2021. Available at: https://www.iec.ch/standards.

[2] M. V. Khenkin, E. A. Katz, A. Abate, G. Bardizza, J. J. Berry, C. Brabec, F. Brunetti, V. Bulović, Q. Burlingame, A. Di Carlo, R. Cheacharoen, Y.-B. Cheng, A. Colsmann, S. Cros, K. Domanski, M. Dusza, C. J. Fell, S. R. Forrest, Y. Galagan, F. Di Giacomo, M. Grätzel, S. Grini, A. Hagfeldt, E. von Hauff, H. Hoppe, J. Kettle, V. Khenkin, D. Kiraç, S. Ko, M. S. Leite, M. Lira-Cantu, S. F. Liu, J. López-Vidrier, J. M. Luther, C.-H. Ma, M. Madsen, M. Manceau, M. Matheron, M. D. McGehee, R. Meitzner, M. K. Nazeeruddin, A. F. Nogueira, Ö. Odabaş, A. Osherov, N.-G. Park, M. O. Reese, F. De Rossi, M. Saliba, U. S. Schubert, H. J. Snaith, S. D. Stranks, W. Tress, P. A. Troshin, V. Turkovic, S. Veenstra, I. Visoly-Fisher, A. Walsh, T. Watson, H.-B. Xie, R. Yıldırım, S. M. Zakeeruddin, K. Zhu, and J. A. A. López, “Consensus statement for stability assessment and reporting for perovskite photovoltaics based on isos procedures,” *Nature Energy*, vol. 5, pp. 35–49, 2020.

[3] International Electrotechnical Commission, “IEC 60904-9:2020: Photovoltaic devices - Part 9: Classification of solar simulator characteristics,” 2020. Available at: https://www.iec.ch/standards.

[4] L. B. Veldscholte and S. de Beer, “Openhumidistat: Humidity-controlled experiments for everyone,” *HardwareX*, vol. 11, p. e00288, 2022.

[5] M. G. Christoforo and J. M. Ball, “centralcontrol,” 2025. Available at https://github.com/greyltc/centralcontrol, accessed March 10, 2025.